INTERNATIONAL JOURNAL FOR NUMERICAL METHODS IN FLUIDS
Int. J. Numer. Meth. Fluids 2009; **60**:1351–1377
Published online 4 December 2008 in Wiley InterScience (www.interscience.wiley.com). DOI: 10.1002/fld.1939

Time step restrictions for well-balanced shallow water solutions in non-zero velocity steady states

J. Murillo[1], P. García-Navarro[1,*,†] and J. Burguete[2]

[1]*Fluid Mechanics, CPS, University of Zaragoza, Spain*
[2]*Soil and Water, EEAD, CSIC, Spain*

SUMMARY

Numerical models based on the conservative formulation of the shallow water equations in finite volumes have recently paid special attention to the convenience of a unified discretization of bed slope source terms and pressure momentum fluxes in order to ensure a correct representation of both in steady states. In cases of steady shallow water flow with non-zero velocity, the discrete balance must include the friction term and the good equilibrium of the discrete solution must be revisited. Besides, there is the question of stability. The presence of relatively large friction terms reduces considerably the stability region of the explicit schemes (with either separate or unified discretization). Implicit formulations strongly help to relax the friction related stability restrictions but are only feasible in the context of separated discretization. Therefore, a strategy to blend both approaches (unified explicit and separated implicit) is presented that ensures both a perfect balance in steady state and numerical stability in unsteady cases in the presence of friction terms. Copyright © 2008 John Wiley & Sons, Ltd.

Received 5 May 2008; Revised 2 September 2008; Accepted 2 September 2008

KEY WORDS: finite volumes; unstructured grids; friction term; explicit discretization; implicit discretization; numerical stability; well-balanced solution

1. INTRODUCTION

Gravity and friction are the main forces driving open channel flows. When using the shallow water model in hydraulic simulation, these forces participate in the dynamic equation as sources/sinks of momentum. Due to the shallow water model hypothesis [1] the gravity force is responsible for both the vertical pressure distribution and the longitudinal water body weight components. In the conservative formulation of the shallow water equations the pressure terms are formulated as dependent on the water depth spatial changes and are included in the definition of the momentum

*Correspondence to: P. García-Navarro, Fluid Mechanics, CPS, University of Zaragoza, Spain.
†E-mail: pigar@unizar.es

Contract/grant sponsor: Spanish Ministry of Science and Education; contract/grant number: CGL2005-07059-C02-02

flux. Numerical models based on the conservative formulation of the shallow water equations in finite volumes have recently paid special attention to the convenience of a unified discretization of bed slope source terms and pressure momentum fluxes in order to ensure a correct representation of both in steady states [2–5]. The so-called C-property [6, 7] was first stated in the context of finite volume methods for the conservative shallow water equations as a required condition for numerical schemes well suited to reproduce the discrete double action of the gravitational force in motionless volumes of water. In cases of steady shallow water flow with non-zero velocity, the pressure and bed slope gravity related terms must be balanced with the friction term and the good equilibrium of the discrete solution must be revisited.

The mathematical modeling of the friction term is commonly done using semi-empirical formulae derived from steady cases and low relative roughness that are open to improved formulations [8] and supported by laboratory experimentation. Independent of the friction model chosen, when moving to the discrete level, numerical experimentation tells us that careless discretization of such formulae may lead to a wrong equilibrium in steady state [9] and to oversize and inadequate values for the discrete friction forces, specially in wet/dry fronts [9–11] that can interfere with the stability of the numerical solution. The current and recommended tendency to avoid numerical errors (lack of balance in the solution and/or oscillations) arising from the friction terms is the remedy of using an implicit treatment of the source term. However, even though implicit discretization of the friction terms may ensure the stability of the numerical solution, a detailed analysis shows that, in steady state, this discretization will never produce an exact balance among fluxes and source terms [12]. It has been proved in one-dimensional (1D) shallow water models that the unified treatment [9] of all the terms, including the friction source term is the only way to ensure Property-C [13] even in steady cases with non-zero velocity. As this treatment is done explicitly, it must be supplied with a condition over the maximum cell dimensions [9] or over the maximum allowable time step [12] in order to guarantee stability.

Recently, [9] a method where the friction source term was truncated when necessary to avoid oscillations in order to avoid restrictions over the cell size or over the time step size was developed. This technique was based on the idea that friction alone can, at most, stop the fluid during one time step but never change the sign of the discharge. This concept cannot be easily extrapolated to the two-dimensional (2D) approach, as there is not a main direction, and also because the grid/time step size reduction can lead to poor computational efficiency in practical applications.

For these reasons it is desirable to find a technique that ensures both a perfect balance in steady state and numerical stability in unsteady cases in the presence of non-zero velocities and friction terms. A technique that combines the implicit pointwise and the explicit upwind friction discretization is proposed in this work trying to achieve computationally efficient simulations. First, the mathematical model will be presented together with two possible friction term formulations. Then, the finite volume numerical technique will be outlined and the two options for implicit pointwise or explicit upwind friction term discretization will be presented and compared using some steady-state open channel flow test cases. One unsteady test case of tsunami run-up will be used to illustrate the technique proposed.

2. MATHEMATICAL MODEL/GOVERNING EQUATIONS

The 2D shallow water equations, which represent mass and momentum conservation in a plane, can be obtained by depth averaging the Navier–Stokes equations. Neglecting diffusion of momentum

DOI: 10.1002/fld

due to viscosity and turbulence, wind effects and the Coriolis term, they form a system of equations [14]:

$$\partial_t \mathbf{U} + \partial_x \mathbf{F}(\mathbf{U}) + \partial_y \mathbf{G}(\mathbf{U}) = \mathbf{S}(\mathbf{U}, x, y) \tag{1}$$

with

$$\begin{aligned} \mathbf{U} &= (h, q_x, q_y)^{\mathrm{T}} \\ \mathbf{F} &= \left(q_x, \frac{q_x^2}{h} + \frac{gh^2}{2}, \frac{q_x q_y}{h} \right)^{\mathrm{T}}, \quad \mathbf{G} = \left(q_y, \frac{q_x q_y}{h}, \frac{q_y^2}{h} + \frac{gh^2}{2} \right)^{\mathrm{T}} \\ \mathbf{S} &= (0, gh(S_{ox} - S_{fx}), gh(S_{oy} - S_{fy}))^{\mathrm{T}} \end{aligned} \tag{2}$$

where h represents the water depth, $q_x = uh$ and $q_y = vh$, with (u, v) the depth-averaged components of the velocity vector $\mathbf{u}$ along the x and y coordinates respectively, g is the acceleration of the gravity, S_{ox} and S_{oy} and S_{fx} and S_{fy} are the bed slopes and friction loss slopes, respectively, along the coordinate directions.

Calling $\mathbf{E} = (\mathbf{F}, \mathbf{G})^{\mathrm{T}}$ (1) becomes:

$$\partial_t \mathbf{U} + \nabla \mathbf{E}(\mathbf{U}) = \mathbf{S} \tag{3}$$

Several formulations for the friction slope term can be found in the literature [8]; in general they can be written as

$$S_{fx} = C_1 u \frac{\sqrt{u^2 + v^2}}{h^{\chi+1}}, \quad S_{fy} = C_1 v \frac{\sqrt{u^2 + v^2}}{h^{\chi+1}} \tag{4}$$

That corresponds to the Glauker–Manning model with $C_1 = n^2$, n being the friction coefficient and χ equal to $\frac{1}{3}$ [15].

3. FINITE VOLUME MODEL

The finite volume scheme used is based on the integration of (3) in a volume or grid cell Ω:

$$\frac{\partial}{\partial t} \int_\Omega \mathbf{U}(x, y)\, \mathrm{d}\Omega + \int_\Omega \nabla \mathbf{E}\, \mathrm{d}\Omega = \int_\Omega \mathbf{S}\, \mathrm{d}\Omega \tag{5}$$

and in the application of Gauss theorem to the second and third integrals. For that purpose, it is assumed that the third integral can be reformulated as [16]

$$\int_\Omega \mathbf{S}\, \mathrm{d}\Omega = \oint_{\partial\Omega} \mathbf{T}^* \mathbf{n}\, \mathrm{d}l \tag{6}$$

where $\mathbf{T}^*$ is a suitable numerical source matrix. This enables the following formulation:

$$\frac{\partial}{\partial t} \int_\Omega \mathbf{U}(x, y)\, \mathrm{d}\Omega + \oint_{\partial\Omega} (\mathbf{E} - \mathbf{T}^*) \mathbf{n}\, \mathrm{d}l = 0 \tag{7}$$

When the domain is sub-divided in cells Ω_i in a mesh fixed in time, (7) can also be applied to each cell (Figure 1).

DOI: 10.1002/fld

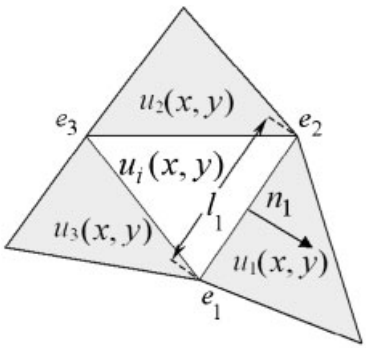

Figure 1. Cell parameters.

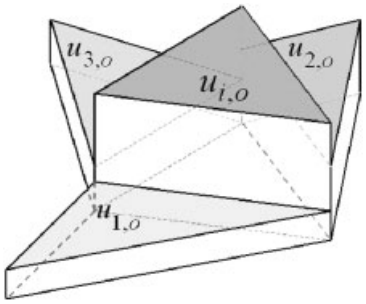

Figure 2. Piecewise constant representation of the variable u.

3.1. First-order schemes

In first-order approach, the vector quantities $\mathbf{U}, \mathbf{E}$ and z are uniform per cell (Figure 2). In particular, the first integral in (7) can be approximated by:

$$\frac{\partial}{\partial t}\int_{\Omega_i}\mathbf{U}(x,y)\,\mathrm{d}\Omega=\frac{\partial \mathbf{U}_i}{\partial t}A_i\cong\frac{\mathbf{U}_i^{n+1}-\mathbf{U}_i^n}{\Delta t}A_i \tag{8}$$

Calling $\mathbf{U}_i(x,y)$ the discrete value of the function $\mathbf{U}$ at cell i and assuming that each cell is surrounded by a set of edges defined by the edge vertices e_k, and the second integral in (7) can be rewritten in a first-order approximation considering the fluxes affecting cell i as:

$$\sum_{k=1}^{NE}\int_{e_k}^{e_{k+1}}(\delta\mathbf{E}(x,y)-\mathbf{T}^*(x,y))_k\mathbf{n}_k\,\mathrm{d}l=\sum_{k=1}^{NE}((\delta\mathbf{E}-\mathbf{T}^*)\mathbf{n}l)_k^n \tag{9}$$

with $\delta\mathbf{E}_k=\mathbf{E}_j-\mathbf{E}_i$ and $\mathbf{T}_k^*$ to be defined.

The flux $\mathbf{E}=\mathbf{E}(\mathbf{U})$ is a nonlinear function but a local linearization of the projection of this flux onto a given direction is possible by means of the definition of an approximated flux Jacobian,

DOI: 10.1002/fld

$\widetilde{\mathbf{J}}_{\mathbf{n},k}$ [17] so that $\delta\mathbf{E}\cdot\mathbf{n}_k=\widetilde{\mathbf{J}}_{\mathbf{n},k}\delta\mathbf{U}_k$, which can be made diagonal

$$\widetilde{\mathbf{J}}_{\mathbf{n},k}=(\widetilde{\mathbf{P}}\widetilde{\mathbf{\Lambda}}\widetilde{\mathbf{P}}^{-1})_k,\quad \widetilde{\mathbf{\Lambda}}_k=(\widetilde{\mathbf{P}}^{-1}\widetilde{\mathbf{J}}_{\mathbf{n}}\widetilde{\mathbf{P}})_k \tag{10}$$

with the help of an eigenvectors-based matrix

$$\widetilde{\mathbf{P}}_k=[\widetilde{\mathbf{e}}^1,\widetilde{\mathbf{e}}^2,\widetilde{\mathbf{e}}^3]_k=\begin{pmatrix}1 & 0 & 1\\ \widetilde{u}+\widetilde{c}n_x & -\widetilde{c}n_y & \widetilde{u}-\widetilde{c}n_x\\ \widetilde{v}+\widetilde{c}n_y & \widetilde{c}n_x & \widetilde{v}-\widetilde{c}n_y\end{pmatrix}_k \tag{11}$$

and with eigenvalues

$$\widetilde{\lambda}^1_{i,k}=(\widetilde{\mathbf{u}}\cdot\mathbf{n}+\widetilde{c})_{i,k},\quad \widetilde{\lambda}^2_{i,k}=(\widetilde{\mathbf{u}}\cdot\mathbf{n})_{i,k},\quad \widetilde{\lambda}^3_{i,k}=(\widetilde{\mathbf{u}}\cdot\mathbf{n}-\widetilde{c})_{i,k} \tag{12}$$

The problem can so be reduced to a 1D Riemann problem projected onto the direction $\mathbf{n}$ at each cell edge [18]. Following a flux difference procedure, the difference in vector $\mathbf{U}$ across the grid edge is projected onto the matrix eigenvectors basis

$$\delta\mathbf{U}_k=\mathbf{U}_j-\mathbf{U}_i=\sum_{m=1}^{3}(\alpha\widetilde{\mathbf{e}})^m_k \tag{13}$$

with

$$\alpha^{1,3}_{i,k}=\frac{\delta h_{i,k}}{2}\pm\frac{1}{2\widetilde{c}_{i,k}}(\delta\mathbf{q}_{i,k}-\widetilde{\mathbf{u}}_{i,k}\delta h_{i,k})\mathbf{n}_{i,k},\quad \alpha^2_{i,k}=\frac{1}{\widetilde{c}_{i,k}}(\delta\mathbf{q}_{i,k}-\widetilde{\mathbf{u}}_{i,k}\delta h_{i,k})\mathbf{n}_{i,k_t} \tag{14}$$

Now the $\delta\mathbf{E}\cdot\mathbf{n}_k$ contributions at a cell edge k can be written as:

$$\delta\mathbf{E}\cdot\mathbf{n}_k=\sum_{k=1}^{NE}\widetilde{\mathbf{J}}_{\mathbf{n},k}\delta\mathbf{U}_k l_k=\sum_{k=1}^{NE}\sum_{m=1}^{3}(\widetilde{\lambda}^m\alpha^m\widetilde{\mathbf{e}}^m)_k l_k \tag{15}$$

The cell edge normal source term $(\mathbf{T}^*\mathbf{n})_k$ is defined as

$$\mathbf{T}^*\mathbf{n}=\begin{pmatrix}0\\ -g\widetilde{h}(\delta z+d_{\mathbf{n}}S_f)n_x\\ -g\widetilde{h}(\delta z+d_{\mathbf{n}}S_f)n_y\end{pmatrix} \tag{16}$$

where the discretization of the friction term at a cell edge in (16) can, for instance, be based on [12]

$$d_{\mathbf{n}}S_{f,k}=d_{\mathbf{n}}C_{1,k}\frac{\widetilde{\mathbf{u}}\mathbf{n}|\widetilde{\mathbf{u}}|}{\widetilde{h}^{\chi+1}} \tag{17}$$

where $d_{\mathbf{n}}$ is the distance between cell centroids sharing edge k projected onto the $\mathbf{n}$ direction and $C_{1,k}=\frac{1}{2}(C_{1,i}+C_{1,j})$.

The cell edge normal source term $(\mathbf{T}^*\mathbf{n})_k$ can also be expressed in function of the eigenvalues and eigenvectors of $\widetilde{\mathbf{J}}_{\mathbf{n},k}$, using the approximate matrix $\widetilde{\mathbf{P}}_k$ [17] in order to reach a unified

DOI: 10.1002/fld

formulation [19]:

$$\mathbf{T}_k^*\mathbf{n}_k=\sum_{m=1}^{N\lambda}(\beta\widetilde{\mathbf{e}})_k^m l_k,\quad \boldsymbol{\beta}_k=\widetilde{\mathbf{P}}^{-1}(\mathbf{T}^*\mathbf{n})_k \tag{18}$$

with $\boldsymbol{\beta}_k=[\beta^1,\beta^2,\beta^3]_k^{\mathrm{T}}$. The coefficients, using (16), are

$$\beta_k^1=-\frac{\widetilde{c}_k}{2}(\delta z_+ d_{\mathbf{n}}S_f)_k,\quad \beta_k^3=-\beta_k^1,\quad \beta^2=0 \tag{19}$$

For the updating algorithm of a given cell i only the in-going contributions generated at the edges are of interest. Finally, the first-order upwind scheme of (7) using a unified discretization gets the form:

$$\mathbf{U}_i^{n+1}=\mathbf{U}_i^n-\sum_{k=1}^{NE}\sum_{m=1}^{3}((\widetilde{\lambda}^-\alpha-\beta^-)\widetilde{\mathbf{e}})_k^m l_k\frac{\Delta t}{A_i} \tag{20}$$

where $\lambda^-=\frac{1}{2}(\lambda-|\lambda|)$ and $\beta^{m-}=\frac{1}{2}(1-\mathrm{sign}(\widetilde{\lambda}^m))\beta^m$. It must be stressed that this form is specially built to ensure well-balanced solutions in both zero and non-zero velocity steady states. We shall refer to this form of friction discretization as unified explicit discretization (UED).

Another formulation using a pointwise evaluation for the friction terms [20] can be used. Splitting the source term $\mathbf{S}(\mathbf{U})$ as the sum of the bottom term $\mathbf{S}_b(\mathbf{U})$ and the roughness–friction term $\mathbf{S}_r(\mathbf{U})$

$$\mathbf{S}(\mathbf{U})=\mathbf{S}_b(\mathbf{U})+\mathbf{S}_r(\mathbf{U}) \tag{21}$$

The numerical scheme is based on an upwind discretization of $\mathbf{S}_b(\mathbf{U})$ and a separated discretization of $\mathbf{S}_r(\mathbf{U})$. This can be summarized as follows:

$$\mathbf{U}_i^*=\mathbf{U}_i^n-\sum_{k=1}^{NE}\sum_{m=1}^{3}((\widetilde{\lambda}^-\alpha-\beta_b^-)\widetilde{\mathbf{e}})_k^m l_k\frac{\Delta t}{A_i} \tag{22}$$

$$\mathbf{U}_i^{n+1}=\mathbf{U}_i^*+\mathbf{S}_r(\mathbf{U}_i^n)\Delta t \tag{23}$$

where the coefficients β_b^- are as in (19) but only include the bottom slope. The second step as in (23) represents a central explicit discretization of $\mathbf{S}_r(\mathbf{U})$. We shall refer to this form of friction discretization as separated explicit discretization (SED).

Alternatively, it can be made implicit in order to reduce numerical instabilities by means of

$$h_i^{n+1}=h_i^*,\quad (hu)_i^{n+1}=(hu)_i^*\frac{1}{1+g(S_{fx}u^{-1})_i^*\Delta t}(hv)_i^{n+1}=(hv)_i^*\frac{1}{1+g(S_{fy}v^{-1})_i^*\Delta t} \tag{24}$$

We shall refer to this form of friction discretization as separated implicit discretization (SID). It is worth remarking that (22) supplied with either (23) or (24) is a formulation unable to provide a correct non-zero velocity steady state as fluxes and source terms are not perfectly balanced.

3.2. Second-order schemes

The spatial accuracy of the scheme can be increased by using piecewise linear instead of piecewise constant representations of the different conserved variables at the cells. Figure 3 is a sketch of

DOI: 10.1002/fld

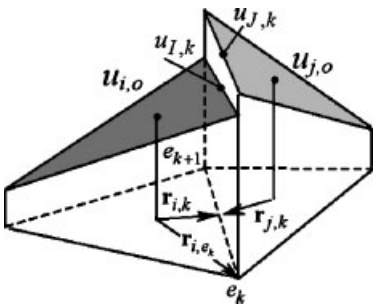

Figure 3. Linear representation by cell.

this idea in the context of triangular grid cells. New values of the conserved variables must be calculated at the cell edges by means of suitable limited procedures [21].

The MUSCL-Hancock scheme extended to systems of equations can be formulated as based on two steps. In the first step the solution must be reconstructed using gradient vectors and then intermediate values are re-calculated at a half time step at cell edges as:

$$\mathbf{U}_{I,k}^{n+1/2} = \mathbf{U}_{I,k}^{n} - \sum_{k=1}^{NE} (\delta \mathbf{E}\mathbf{n}_k - \mathbf{T}^* \mathbf{n}_k)_{Ii,k}^{n} \frac{l_k}{A_i} \frac{\Delta t}{2} \tag{25}$$

The updated variable is constructed as

$$\mathbf{U}_{i}^{n+1} = \mathbf{U}_{i}^{n} - \sum_{k=1}^{NE} (\delta \mathbf{E}\mathbf{n}_k - \mathbf{T}^* \mathbf{n}_k)_{JI,k}^{n+1/2,-} \frac{l_k}{A_i} \Delta t - \sum_{k=1}^{NE} (\delta \mathbf{E}\mathbf{n}_k - \mathbf{T}^* \mathbf{n}_k)_{Ii,k}^{n+1/2} \frac{l_k}{A_i} \Delta t \tag{26}$$

where $\delta \mathbf{E}_{JI,k}^{n+1/2} = \mathbf{E}_{J,k}^{n+1/2} - \mathbf{E}_{I,k}^{n+1/2}$ and $\delta \mathbf{E}_{Ii,k}^{n+1/2} = \mathbf{E}_{I,k}^{n+1/2} - \mathbf{E}_{i,k}^{n}$, with an upwind part (first term) and a central part (second term).

It is important to remark that, in order to enforce the good balance, when making the interpolation planes it is necessary to interpolate over the water level surface to ensure equilibrium in still water steady cases. More details can be found in [21]. The scheme as in (25) and (26) closely follows the unified discretization leading to the first-order scheme (20).

Alternatively, it is also possible to build an extension to second order in which the friction terms are discretized separately. This will be formulated in three steps as follows:

$$\mathbf{U}_{I,k}^{n+1/2} = \mathbf{U}_{I,k}^{n} - \sum_{k=1}^{NE} (\delta \mathbf{E}\mathbf{n}_k - \mathbf{T}_b^* \mathbf{n}_k)_{Ii,k}^{n} \frac{l_k}{A_i} \frac{\Delta t}{2} \tag{27}$$

$$\begin{aligned} \mathbf{U}_{i}^{*} &= \mathbf{U}_{i}^{n} - \sum_{k=1}^{NE} (\delta \mathbf{E}\mathbf{n}_k - \mathbf{T}_b^* \mathbf{n}_k)_{JI,k}^{n+1/2,-} \frac{l_k}{A_i} \Delta t - \sum_{k=1}^{NE} (\delta \mathbf{E}\mathbf{n}_k - \mathbf{T}_b^* \mathbf{n}_k)_{Ii,k}^{n+1/2} \frac{l_k}{A_i} \Delta t \\ \mathbf{U}_{i}^{n+1} &= \mathbf{U}_{i}^{*} + \mathbf{S}_r(\mathbf{U}_{i}^{n}) \Delta t \end{aligned} \tag{28}$$

In (27) and (28) $\mathbf{T}_b^*$ makes reference only to the bottom variation source terms.

DOI: 10.1002/fld

Following an implicit formulation, the last step will be:

$$h_i^{n+1}=h_i^*,\quad (hu)_i^{n+1}=(hu)_i^*\frac{1}{1+f_i^*\Delta t}(hv)_i^{n+1}=(hv)_i^*\frac{1}{1+f_i^*\Delta t} \tag{29}$$

It must be repeated that this formulation is unable to provide a correct steady state as fluxes and source terms are not perfectly balanced.

4. FRICTION TERM STABILITY CONSTRAINTS

Explicit numerical schemes such as those presented in this work are conditionally stable. Courant–Friedrichs–Lewy stated the restrictions on the time step size for a given mesh in case of homogeneous linear partial differential equations (CFL condition) [22]. For a generalization to the shallow water equations in triangular grids see Murillo *et al.* [12]. In this section we are concerned with the additional stability restrictions imposed by a dominant roughness on the numerical scheme used.

According to Murillo *et al.* [12] the SED of the friction terms interferes with the CFL stability condition. The following additional limit on the time step size for both first- and second-order approaches when using a grid of a given mesh size is required:

$$\begin{aligned}&\Delta t=\min\{\Delta t_r,\Delta t_{\mathrm{CFL}}\}\\ &\Delta t_r=\min\left\{\left(\frac{n^2|\mathbf{u}_i|}{h_i^{\chi+1}}g\right)^{-1}\right\}_{i=1,\mathrm{Ncell}},\quad \Delta t_{\mathrm{CFL}}=\min\left\{\frac{A_{\min,k}}{\max_m\{|\widetilde{\lambda}_k^m|\}l_k}\right\}_{k=1,\mathrm{Nedge}}\end{aligned} \tag{30}$$

Otherwise, the stability can only be ensured by refining the grid. Both possibilities offer stability at a high computational cost. This will be shown in the numerical tests section. The SID of the friction term is not time dependent. Therefore, it will not be considered in this section as it does not require further time step restrictions than the CFL condition.

Although the UED of the friction term in (17) is associated with the cell edge, it is not necessary to evaluate it using exclusively edge-averaged values of all quantities. In order to mitigate the over-estimation of the friction slope in singular situations, instead of (17) another approach for the modeling of the friction slope is proposed:

$$d_{\mathbf{n}}S_{f,k}=d_{\mathbf{n}}C_{1,k}\frac{\widetilde{\mathbf{u}}\mathbf{n}u_{\min}}{h_{\max}^{\chi+1}} \tag{31}$$

with $h_{\max}=\max\{h_i,h_j\}$ and $u_{\min}=\min\{|\mathbf{u}_i|,|\mathbf{u}_j|\}$. In order to avoid instabilities, the following condition over the time step Δt_k was proposed [12]:

$$\Delta t=\min\left\{\left(\frac{C_1|\widetilde{\mathbf{u}}|}{\widetilde{h}^{\chi+1}}\frac{d_{\mathbf{n}}l}{A_{\min,k}}g\right)^{-1},\frac{A_{\min,k}}{\max_m\{|\widetilde{\lambda}_k^m|\}l_k}\right\}_{k=1,\mathrm{Nedge}} \tag{32}$$

It is desirable to find a technique that avoids reducing the time step size below the CFL condition in cases of high relative roughness in order to preserve the computational efficiency of the scheme. For that reason, a technique that combines the best properties of the SID and of the UED is

DOI: 10.1002/fld

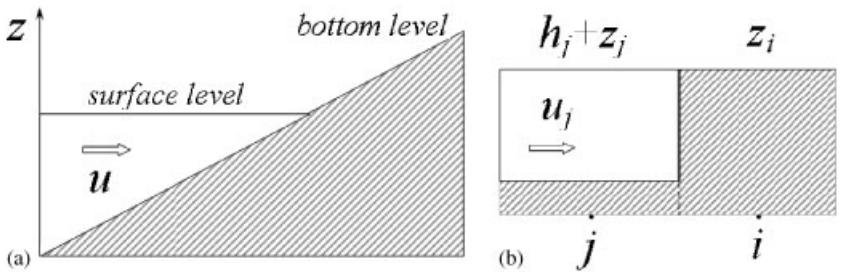

Figure 4. Adverse slope and flat surface level.

proposed in this work, ensuring conservation in all cases. This technique imposes a limit over the size of the friction term when using the UED. When this limit is exceeded the SID of the friction source term is enforced.

The search for the limiting value of discrete friction term stars by requiring that friction alone is not able to change the sign of the discharge; hence, the following condition is enforced over the unit discharge function:

$$(h_i \mathbf{u}_i \mathbf{n})^{n+1} (h_i \mathbf{u}_i \mathbf{n})^* \geqslant 0 \tag{33}$$

where $\mathbf{n}$ is the normal unit vector to a grid edge.

Friction is dominant in cases of low water depth as shorelines. Such a situation is represented by Figure 4(a), where a flat surface level develops over an adverse slope.

In this situation, the momentum equations are reduced to

$$\begin{aligned} \partial_t(hu) + \partial_x(hu^2) + \partial_y(huv) &= -ghS_{f,x} \\ \partial_t(hv) + \partial_x(huv) + \partial_y(hv^2) &= -ghS_{f,y} \end{aligned} \tag{34}$$

or considering a normal direction $\mathbf{n}$

$$\partial_t(h\mathbf{un}) + \nabla(h\mathbf{u}(\mathbf{un})) = -gh(S_{fx}, S_{fy})^{\mathrm{T}}\mathbf{n} \tag{35}$$

Taking into account (35) the following can be written for a conservative finite volume scheme across an edge k:

$$(h\mathbf{u}_i\mathbf{n}_k)^{n+1} = (h\mathbf{u}_i\mathbf{n}_k)^n - [\delta(h\mathbf{u}(\mathbf{un})) + g\widetilde{h}(S_{f,k}d_{\mathbf{n}})]_k \frac{l_k}{A_i}\Delta t \tag{36}$$

with $\widetilde{h} = \frac{1}{2}(h_i + h_j)$. If the advance is discretized as in Figure 4(b), i being the dry cell ($\mathbf{u}_i^n\mathbf{n}_k = h_i^{n+1} = 0$) and j the wet cell ($\mathbf{u}_j^n\mathbf{n}_k \geqslant 0, h_j^n \geqslant 0$), the following is expected:

$$\mathbf{u}_i^{n+1}\mathbf{n}_k \geqslant 0, \quad h_i^n \geqslant 0 \tag{37}$$

As our main goal is to avoid the possibility of discrete friction terms greater than discrete advection terms, the following condition is required:

$$[(h\mathbf{u}(\mathbf{un}))_j - \tfrac{1}{2}gh_j(|S_{f,k}|d_{\mathbf{n}})]_k \leqslant 0 \tag{38}$$

thus providing the required limit for the use of the upwind formulation.

DOI: 10.1002/fld

Other cases that do not include the presence of wet/dry fronts are also of interest, but (38) can be extended to give a practical rule. In order to consider the most restrictive situation, the following limit is proposed:

$$g\widetilde{h}_k(|S_{f,k}|d_{\mathbf{n},k}) < h_{\min}u^2_{\min} \tag{39}$$

with $h_{\min}=\min\{h_i, h_j\}$. When the inequality (39) does not hold, the SID is applied to both the cells involved.

With this simple mechanism all instabilities likely to appear both in the advance front in flooding events and in steady-state conditions are avoided.

5. NUMERICAL RESULTS

5.1. Circular dam break with friction

This test case of a circular dam break with friction in a flat squared domain was analyzed in [12]. The domain size is $2000\,\mathrm{m}\times 2000\,\mathrm{m}$ and has been discretized in three triangular structured meshes, M1, M2 and M3 using a characteristic length l equal to 80, 50 and 25 m, respectively (Figure 5) in order to evaluate the sensitivity of the friction term discretization strategies to the grid refinement.

With the origin located at the center of the domain, the initial water depth elevation is given by

$$h(r, t=0)=\begin{cases}0.01\,\mathrm{m} & \text{if } r>800\,\mathrm{m}\\ 5\,\mathrm{m} & \text{if } r\leqslant 800\,\mathrm{m}\end{cases} \tag{40}$$

with r the radial distance from the center of the domain. The friction has been modeled considering a Manning's roughness parameter $n=0.05\,\mathrm{sm}^{-1/3}$.

Meshes M1 and M2 have been chosen to show the inefficiency of the CFL condition to control numerical stability in this case. The computation, when based only on the CFL condition, blows up at approximately $t=20\,\mathrm{s}$ when using UED and approximately at $t=10\,\mathrm{s}$ when using the SED in mesh M1 as Figures 6(a) and 7(a) display. This numerical instability, generated by the friction term, can be avoided by means of more restrictive time step conditions as said before. Figures 6(b) for the UED and 7(b) for the SED show the stabilized solution when applying (32) and (30), respectively. Alternatively, a stable solution is also provided by the proposed hybrid method as 6(c) and 7(c) show. Figure 8 represents the water surface level at $t=40\,\mathrm{s}$ from the four stabilized

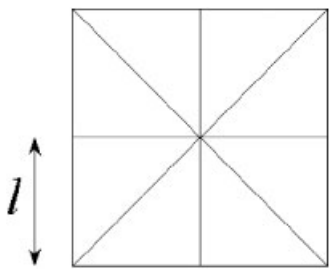

Figure 5. Cell discretization.

DOI: 10.1002/fld

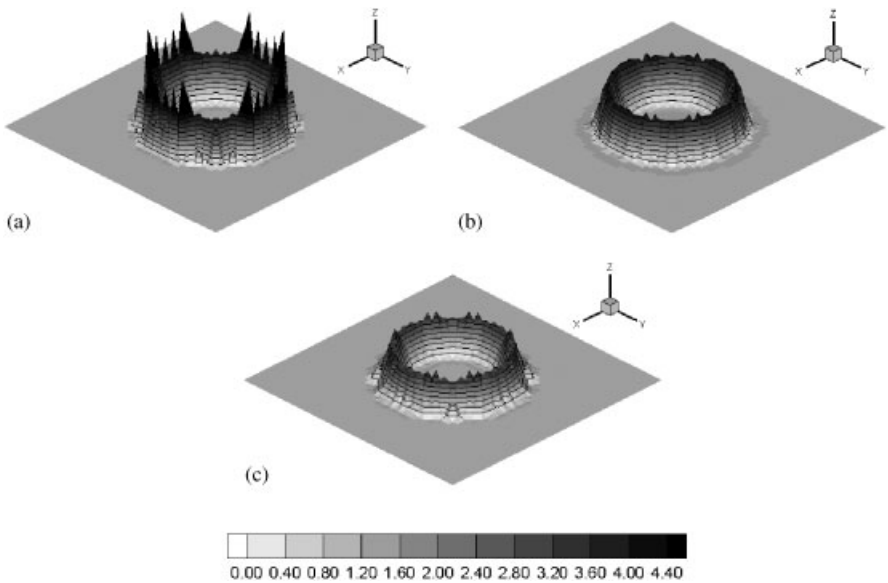

Figure 6. 3D contour plot of the velocity module in mesh M1 at $t = 20$ s using: (a) the UED only with the CFL condition; (b) the UED with the extra time step restriction (34); and (c) the hybrid method.

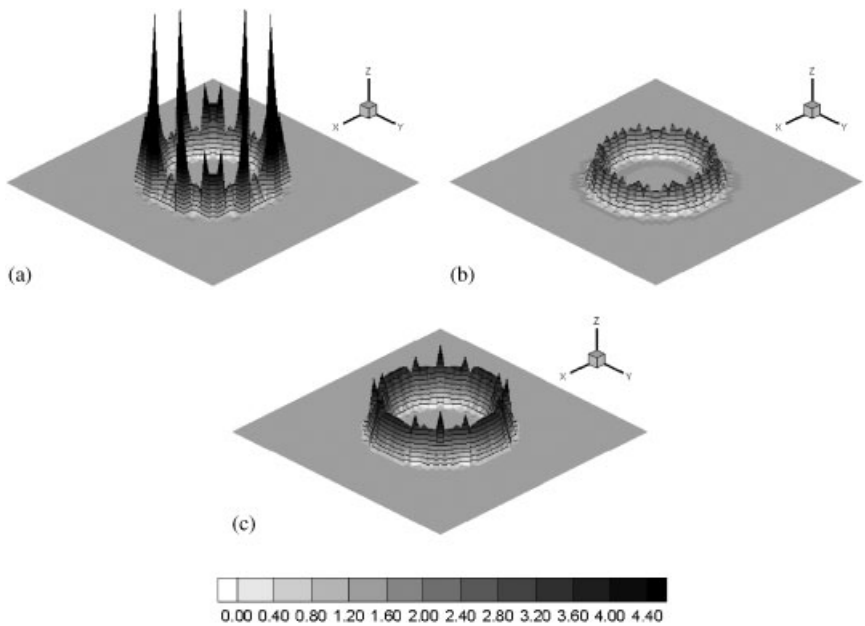

Figure 7. 3D contour plot of the velocity module in mesh M1 at $t = 10$ s using: (a) the SED only with the CFL condition; (b) the SED with the extra time step restriction (31); and (c) the hybrid method.

DOI: 10.1002/fld

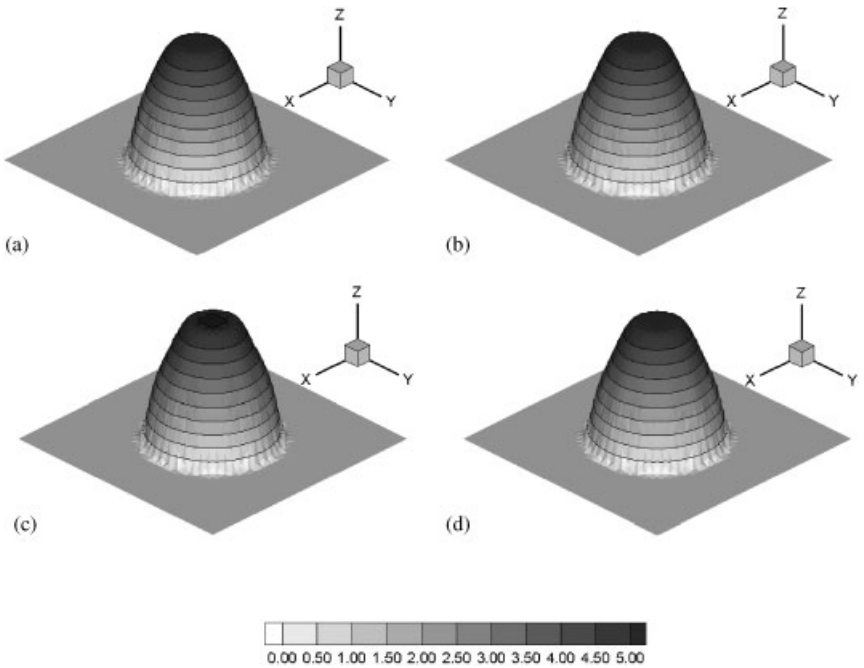

Figure 8. 3D contour plot of the water level surface in mesh M1 at $t = 40$ s using: (a) the UED with the extra condition (34); (b) the SED with the extra time step restriction (31); (c) the SID with CFL condition; and (d) the hybrid method.

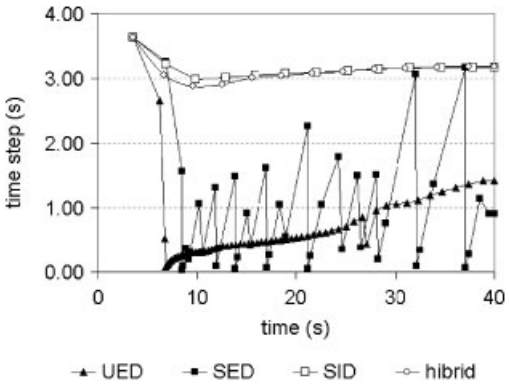

Figure 9. Time step evolution in M1.

methods on mesh M1. Figure 8(a) is the UED with the extra condition (32), Figure 8(b) corresponds to the SED with the extra time step restriction (31), Figure 8(c) is the SID with the CFL condition and Figure 8(d) is the hybrid method. The most important feature is that all four provide the same accuracy in this case. The important point is that there is a noticeable difference among the

DOI: 10.1002/fld

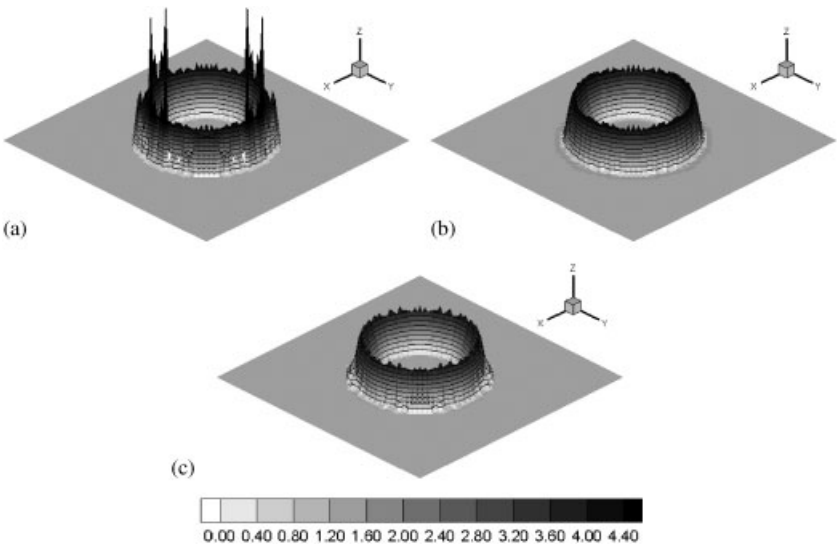

Figure 10. 3D contour plot of the velocity module in mesh M2 at $t = 15$ s using: (a) the UED only with the CFL condition; (b) the UED with the extra time step restriction (34); and (c) the hybrid method.

methods in the size and uniformity of the time step size required to achieve stable results. This is displayed in Figure 9.

The computation, when based only on the CFL condition blows up at approximately $t = 15$ s when using UED and approximately at 10 s when using the SED in mesh M2 as Figures 10(a) and 11(a) display. Figure 10(b) for the UED and Figure 11(b) for the SED show the stabilized solution when applying (32) and (30), respectively. The proposed hybrid method is shown in Figures 10(c) and 11(c). Figure 12 represents the water surface level at $t = 40$ s from the four stabilized methods on mesh M2. The same comments as those in the previous paragraph can be made. Figure 13 compares the size and uniformity of the time step size used by each method.

Figure 14 corresponds to the water surface levels calculated by the four stabilized schemes in mesh M3 at time $t = 40$ s. It must be noted, however, that this mesh is fine enough to provide stable solutions under the sole CFL condition with all the friction discretization techniques. Figure 15 displays the size and uniformity of the time step used by the UED with condition (32), SED with condition (30), SID and hybrid techniques for comparison purposes.

5.2. *Channel contraction*

Despite the superiority shown by the friction SID in the previous test case as far as stability is concerned, a further analysis of the relative performance of the methodologies in steady state is necessary in order to evaluate their ability to produce a well-balanced solution. In order to see the importance of the balance of the pressure, slope and friction terms and, at the same time, be able to define a highly variable steady flow, a sloping ($S_{ox} = 0.001$ m/m) rectangular open channel with a sharp contraction in the middle is considered. The channel is 110 m long and 10 m wide. A symmetrical contraction located 50 m downstream the inlet boundary is assumed, reducing the section width to 1 m (Figure 16(a)). A constant discharge of $40\,\mathrm{m}^3/\mathrm{sg}$ is set at the upstream

DOI: 10.1002/fld

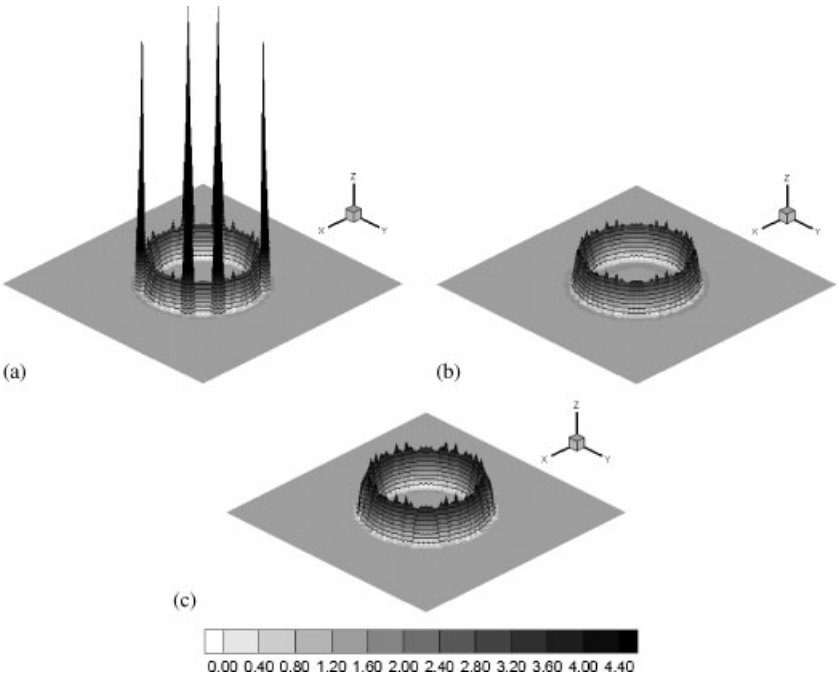

Figure 11. 3D contour plot of the velocity module in mesh M2 at $t = 10$ s using: (a) the SED only with the CFL condition; (b) the SED with the extra time step restriction (31); and (c) the hybrid method.

boundary and free flow is assumed at the downstream boundary. The simulation is performed starting from dry bed initial conditions. A Manning friction coefficient $n = 0.03$ is assigned to the entire channel. The domain is discretized using two coarse triangular meshes, M1 and M2, of characteristic length $l = 1$ m and 0.5 m, respectively (Figure 16(b)). This case is interesting for our purposes as it combines strong values of friction slope and strong variations in both the curvature of the water level surface and of the velocity.

Figure 17(a) shows the time evolution of the total discharge at the middle of the narrow section on both grids M1 (left) and M2 (right). Both the UED and the hybrid techniques provide an exact value of water discharge in time while the purely implicit SID provides a value smaller than the correct one. Figure 17(b) shows the evolution of the discharge in time at the free flowing outlet section. Both the UED and the hybrid techniques provide an exact value of water discharge when steady state is achieved and, as all the fluxes are exactly balanced, the water level surface remains fixed in time. On the other hand, Figure 17(b) shows that the SID method produces oscillations in the solution and is unable to generate a steady solution. This produces strong differences for the water level surface and velocity distribution among the upwind or upwind-implicit techniques and the implicit techniques.

Figure 18 shows the 3D view of the water level surface at time $t = 2000$ s obtained with all the techniques on both grids M1 (left) and M2 (right). Figure 18(a) displays the results using the UED technique. Figure 18(b) represents the results at the same time when using the SED technique where the lack of symmetry in the numerical surface is noticeable on both grids. The same can be said about the solution provided by the SID technique shown in Figure 18(c). Figure 18(d) and (e)

DOI: 10.1002/fld

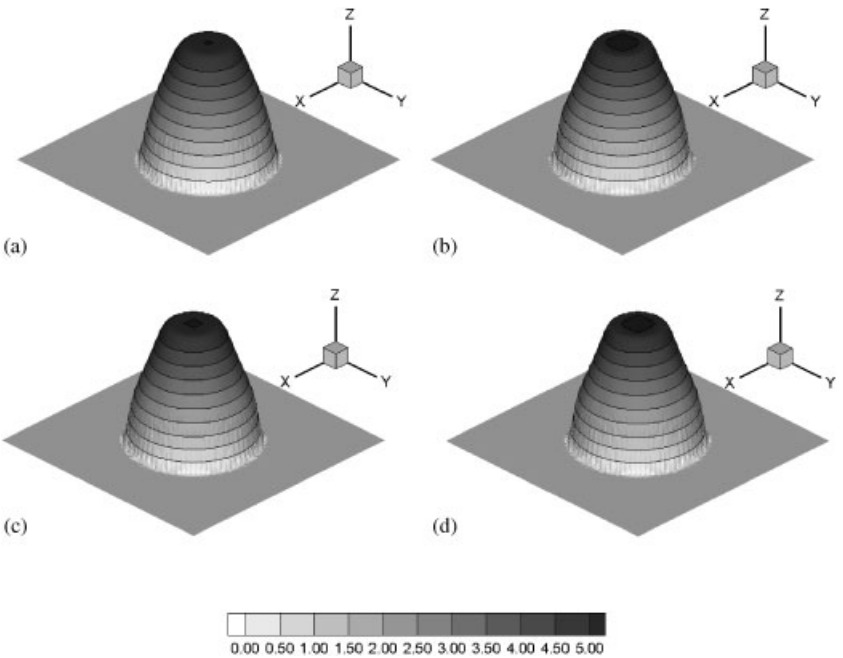

Figure 12. 3D contour plot of the water level surface in mesh M2 at $t = 40$ s using: (a) the UED with the extra condition (34); (b) the SED with the extra time step restriction (31); (c) the SID with CFL condition; and (d) the hybrid method.

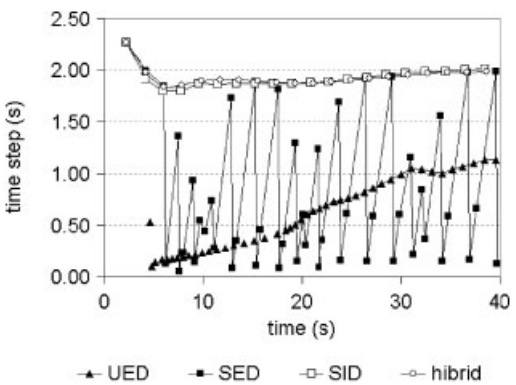

Figure 13. Time step evolution in M2.

shows the solution obtained with the hybrid approach based on a first-order scheme and a second-order scheme, respectively. They are as accurate as the UED solution and have been calculated using larger time steps of smoother distribution in time. Due to the coarseness of both grids and the presence of source terms, the second-order approach does not show a superior accuracy in this case.

DOI: 10.1002/fld

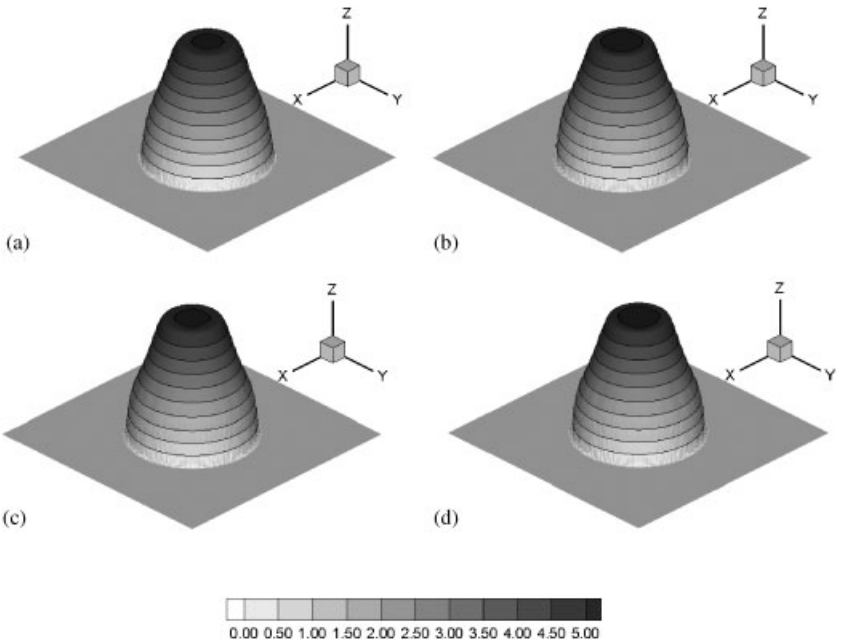

Figure 14. 3D contour plot of the water level surface in mesh M3 at $t = 40$ s using: (a) the UED with the extra condition (34); (b) the SED with the extra time step restriction (31); (c) the SID with CFL condition; and (d) the hybrid method.

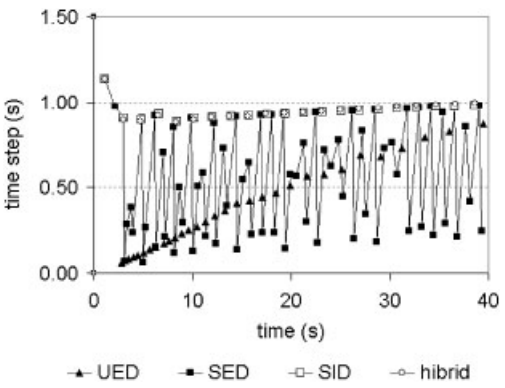

Figure 15. Time step evolution in M3.

The evolution of the time step in this case, Figure 19, shows how the hybrid scheme overcomes the lack of efficiency that arises when using the UED. The use of the pure upwind approach demands a strong reduction in the time step. As a general rule must be applied to ensure stability in all cases, this reduction can be excessive as this case makes plain. Figure 20 shows a detail of the contour plot of the module of the velocity downstream the narrowing region when using the UED

DOI: 10.1002/fld

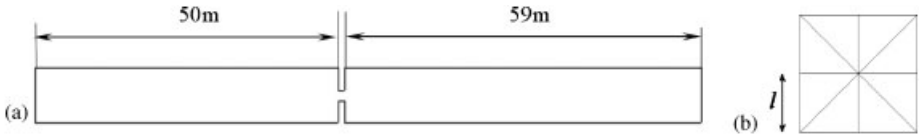

Figure 16. Computational domain (a) and cell discretization (b).

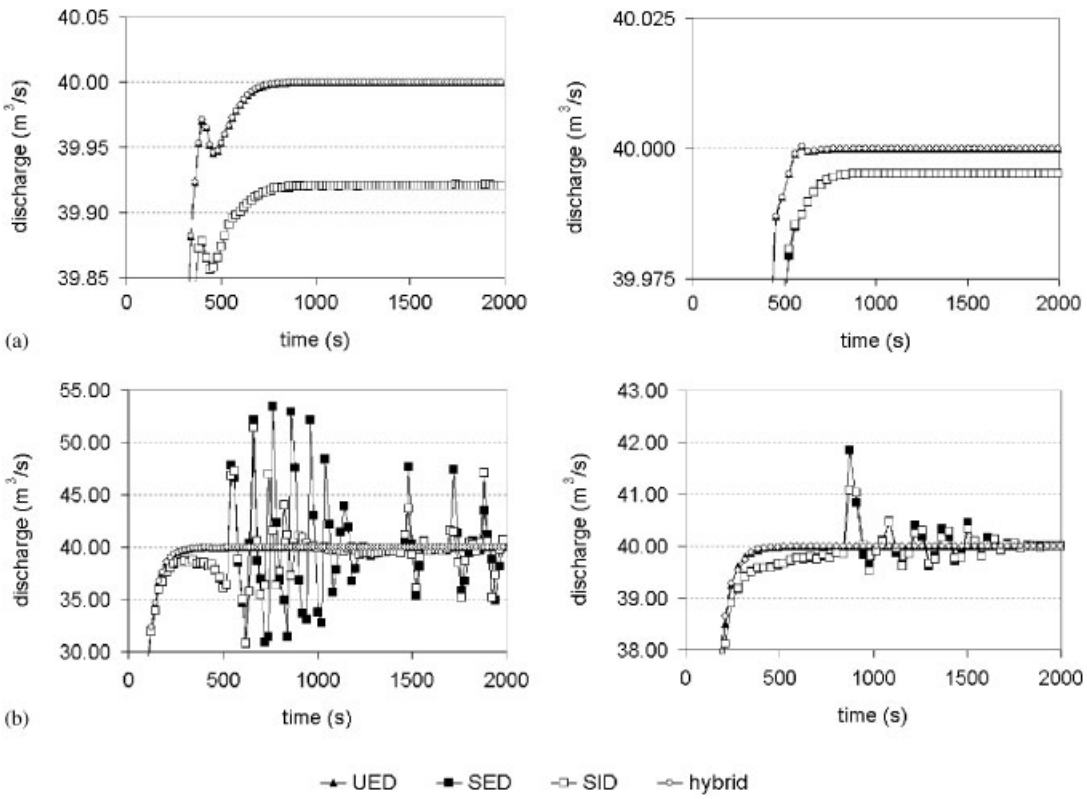

Figure 17. Water discharge time evolution: (a) at the narrow cross section and (b) at the outlet boundary cross section. Left M1 grid and right M2 grid.

(Figure 20(a)) and the hybrid method (Figure 20(b)). Despite the differences in the magnitude of the time step used in each case no differences appear when comparing both results.

5.3. Tsunami wave run-up

This test case has been taken from a benchmark problem of the Third International Workshop on Long Wave Runup Models. It is a 1/400 scale laboratory experiment of the Monai run-up (Okushiri Island, Japan) using a large-scale tank (205 m long, 6 m deep, 3.4 m wide) at the Central Research Institute for Electric Power Industry (CRIEPI) in Abiko, Japan. A benchmark test case was defined focusing on a region near the shoreline where experimental data were measured. The

DOI: 10.1002/fld

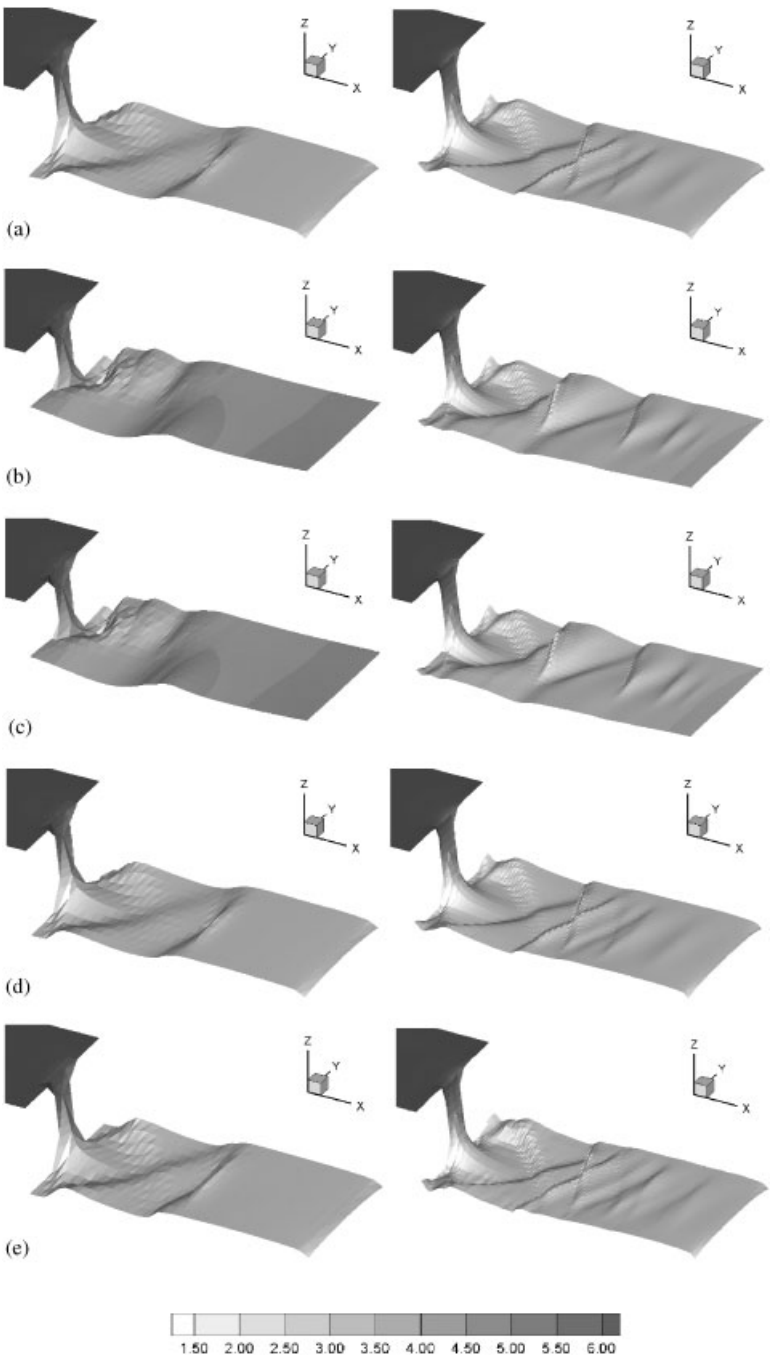

Figure 18. Water level surface at $t = 2000$ s using: (a) the UED; (b) the SED; (c) the SID; (d) the hybrid first-order; and (e) the hybrid second-order approach. Left M1 grid and right M2 grid.

DOI: 10.1002/fld

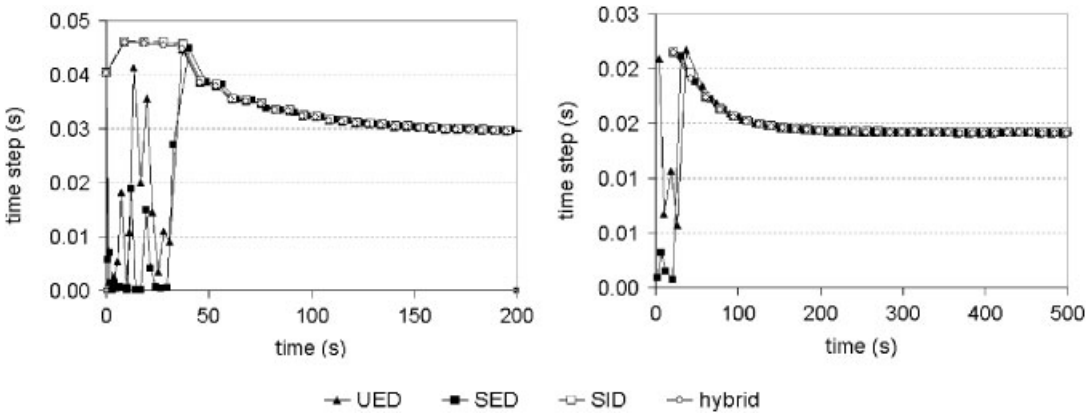

Figure 19. Time step evolution in time.

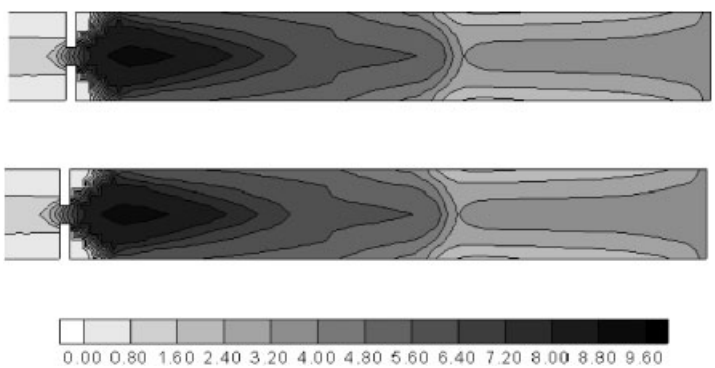

Figure 20. Module of the velocity at time $t=2000\,\mathrm{s}$ using (a) the UED (b) and the hybrid method.

detailed description as well as the experimental data are available [23]. According to the reported bed material we have used a Gauckler–Manning number of $n=0.01\,\mathrm{sm}^{-1/3}$.

This test case has been used to show the numerical solutions obtained in a wide range of grid refinement in order to demonstrate the robustness of the numerical techniques proposed.

Figure 21 represents the bathymetry used in the reduced scale model and the locations of three gauging points ($x=4.52\,\mathrm{m}$ and $y=2.196\,\mathrm{m}$, $y=1.696\,\mathrm{m}$, $y=1.196\,\mathrm{m}$, initially submerged) where the evolution of the water depth was measured. The initial condition is still water with a constant water level surface, $h+z=0\,\mathrm{m}$. The incident wave from offshore appears in the boundary with maximum water depth $h=13.5\,\mathrm{cm}$ ($x=0$), and is defined by means of the variation of the water depth in time, Figure 22. In the laboratory model the other three boundaries were reflective vertical sidewalls and so have been considered in our model.

For the simulation the domain has been discretized using triangular meshes shaped as shown in Figure 5, using a length that varies from $l=0.007\,\mathrm{m}$ to $l=0.224\,\mathrm{m}$. Table I summarizes the resulting computational grids. Figures 23–26 show a sequence of the time evolution of the water surface as the flood wave progresses over the coast. At time $t=12\,\mathrm{s}$ (Figure 23) the depression

DOI: 10.1002/fld

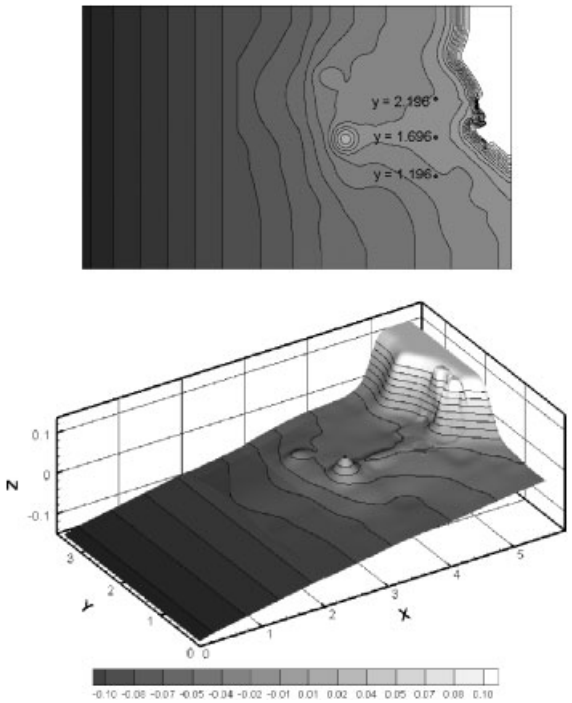

Figure 21. Contour plot of the bathymetry and location of the gauging points.

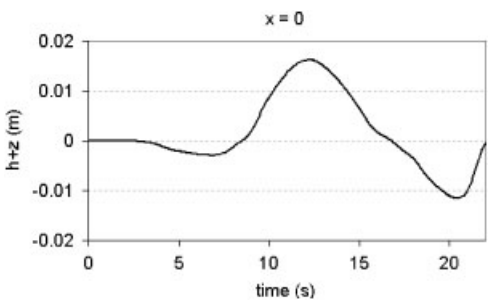

Figure 22. Water level surface time variation at the inlet boundary.

Table I. Number of cells and size cell in each mesh discretization.

	M1	M2	M3	M4	M5	M6
Length l	0.007	0.014	0.028	0.056	0.112	0.224
Cells	762 048	190 512	47 432	11 956	2940	750

DOI: 10.1002/fld

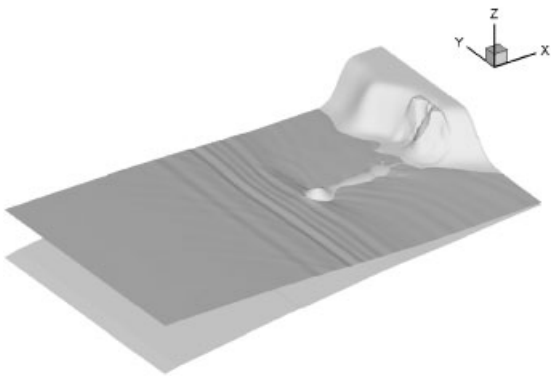

Figure 23. 3D contour plot of the water level surface at time 12 s. The shoreline is moving backward.

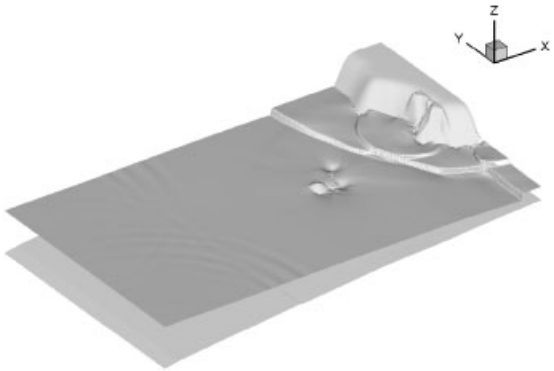

Figure 24. 3D contour plot of the water level surface at time 17 s. The wave has reached the highest point in the shoreline and has been reflected.

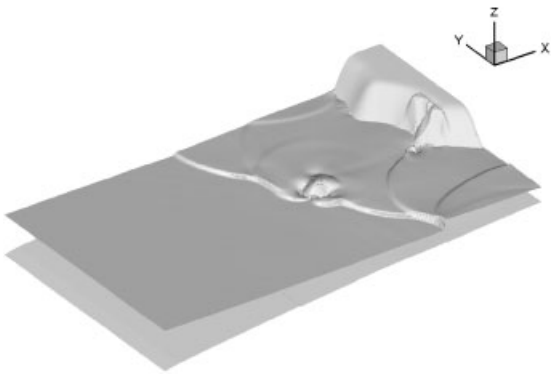

Figure 25. 3D contour plot of the water level surface at time 19 s. The flood wave has covered the small island.

DOI: 10.1002/fld

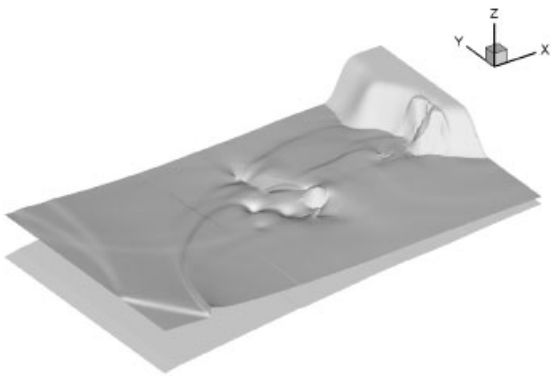

Figure 26. 3D contour plot of the water level surface at time 22 s. The small island can be seen again.

wave makes the shoreline to move backward. At time $t = 17$ s (Figure 24) the inundation wave has reached the highest point in the shoreline and has also been reflected. At time $t = 19$ s (Figure 25) the flood wave has covered the small island. At time $t = 22$ s (Figure 26) the small island can be seen again.

Figure 27 shows the computed time evolution of the water surface level at the three gauging points together with the measurements provided, using meshes M1, M2 and M3. Figure 28 compares the results using M4, M5 and M6. Figure 29 compares the solution using first- and second-order approaches for mesh M1. There are no noticeable differences in the two numerical solutions.

6. CONCLUSIONS

In this work, the numerical modeling of the friction terms within the framework of 2D shallow water upwind finite volume models has been analyzed and various existing forms of discretizing the friction term have been discussed.

The starting point is that in cases of steady shallow water flow with non-zero velocity, the bed slope source terms are not the only to be included in a unified discretization but all the terms in the momentum equation must be balanced with the friction term in order to provide a good equilibrium in the discrete solution. A first conclusion is that only the fully unified discretization ensures a correct non-zero velocity steady state.

As for the stability constraints, when using an explicit upwind scheme both the unified (upwind) and separated (pointwise) explicit discretization of the friction term require an additional time step reduction in cases of dominant roughness. On the other hand, a separated implicit technique for the friction term discretization is useful to relax the condition over the time step since it does not introduce new stability constraints but is unable to ensure a well-balanced steady state.

A technique that combines the implicit pointwise and the explicit upwind friction discretization has been proposed in order to achieve computationally efficient simulations by means of an adequate criterion that is used to switch from one to the other while remaining under the sole control of the CFL time step condition.

The numerical test cases selected have been useful to demonstrate these properties. The numerical solutions obtained with the explicit unified discretization have been used as the reference

DOI: 10.1002/fld

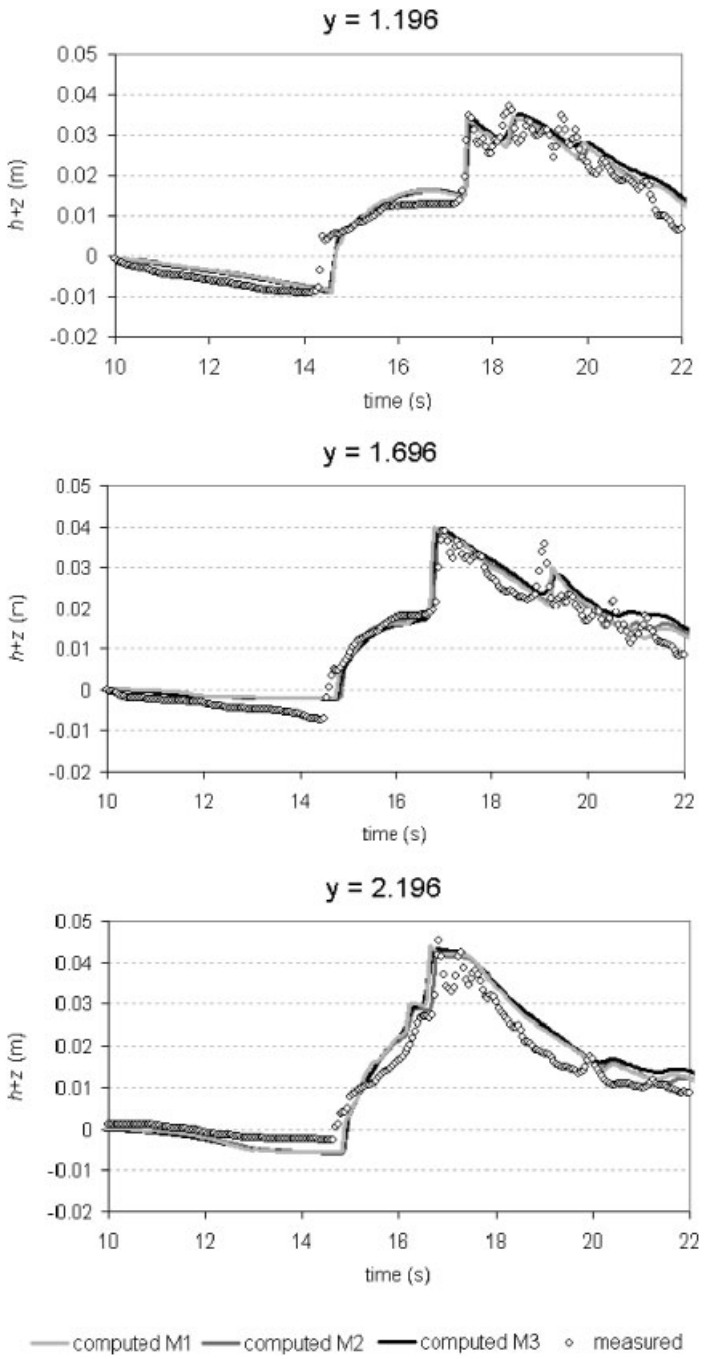

Figure 27. Water level surface variation at the three gauging points using meshes M1, M2 and M3.

DOI: 10.1002/fld

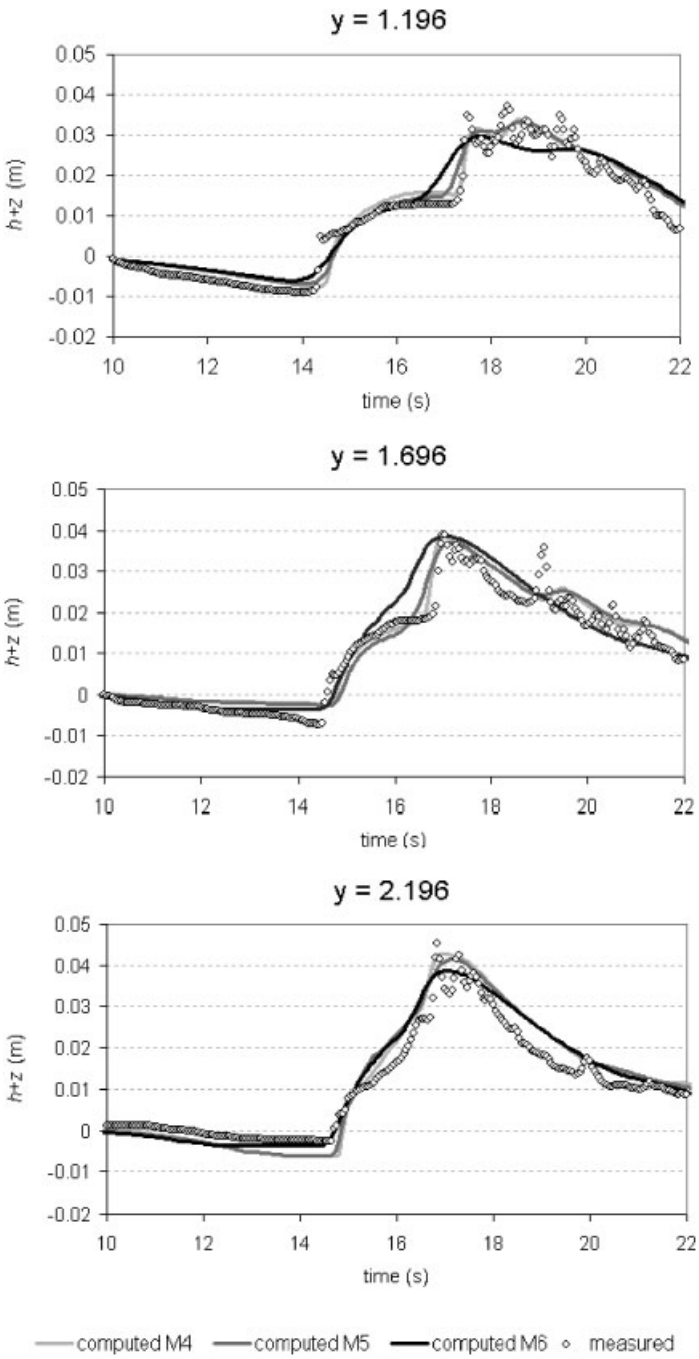

Figure 28. Water level surface variation at the three gauging points using meshes M4, M5 and M6.

DOI: 10.1002/fld

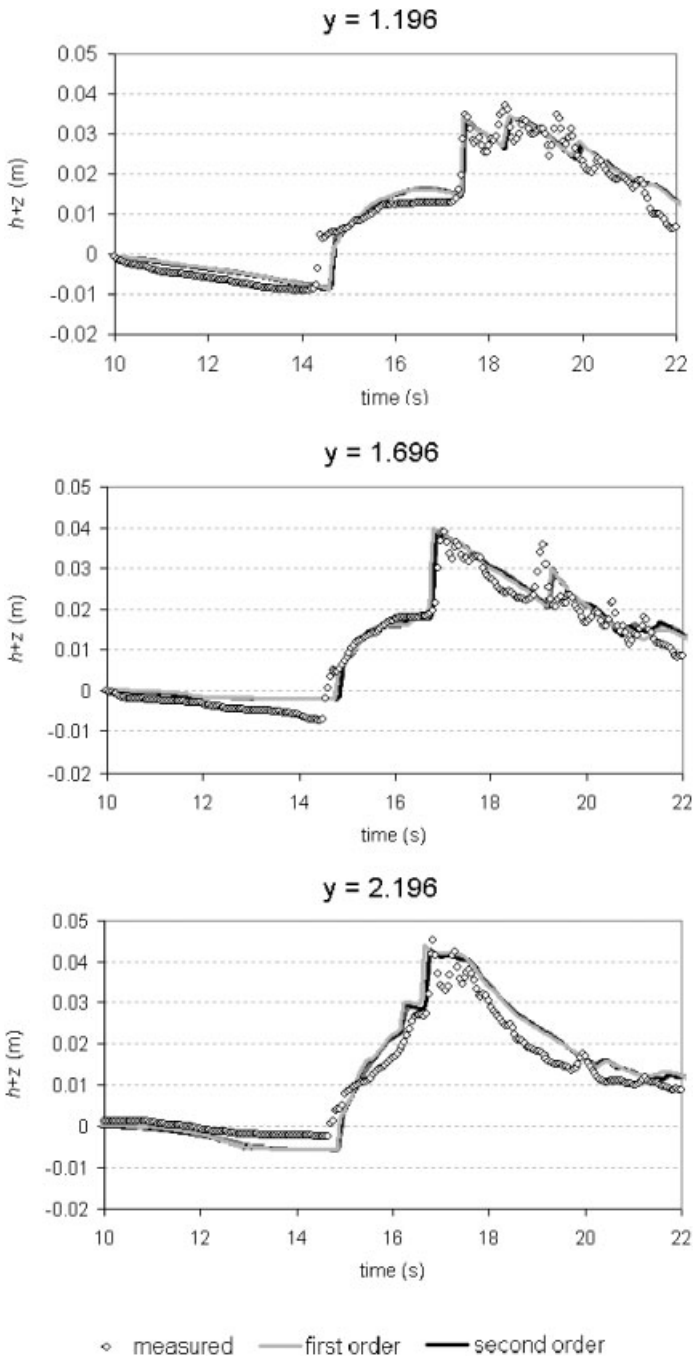

Figure 29. Water level surface variation at the three gauging points using mesh M1 with first- and second-order approach.

DOI: 10.1002/fld

solutions that can only be obtained at a relatively high computational cost. Our results highlight the smoothness of the dynamically calculated time step size achieved by the proposed hybrid technique that, at the same time, retains the accuracy and equilibrium properties of the pure unified discretization. The proposed method can be adapted to both a first-order and a second-order explicit scheme with the same properties.

ACKNOWLEDGEMENTS

This work is a part of the research activities of the project CGL2005-07059-C02-02 funded by the Spanish Ministry of Science and Education.

REFERENCES

1. Cunge JA, Holly FM, Vervey A. *Practical Aspects of Computational River Hydraulics*. Pitman: London, 1980.
2. Hubbard ME, García-Navarro P. Flux difference splitting and the balancing of source terms and flux gradients. *Journal of Computational Physics* 2000; **165**:89–125.
3. LeVeque RJ. Balancing source terms and flux gradients in high-resolution Godunov methods: the quasi-steady wave-propagation algorithm. *Journal of Computational Physics* 1998; **146**(1):346–365.
4. Bradford SF, Sanders BF. Finite-volume model for shallow water flooding of arbitrary topography. *Journal of Hydraulic Engineering* 2002; **128**(3):289–298.
5. Zhou J, Causon DM, Mingham CG, Ingram DM. Numerical prediction of dam-break flows in general geometries with complex bed topography. *Journal of Hydraulic Engineering* (ASCE) 2004; **130**(4):332–340.
6. Bermúdez A, Dervieux A, Desideri JA, Vázquez-Cedón ME. Upwind schemes for the two-dimensional shallow water equations with variable depth using unstructured meshes. *Computer Methods in Applied Mechanics and Engineering* 1998; **155**:49–72.
7. Bermúdez A, Vázquez ME. Upwind methods for hyperbolic conservation laws with source terms. *Computers and Fluids* 1998; **8**:1049–1071.
8. Chow VT. *Open Channel Flow*. McGraw-Hill: New York, 1959.
9. Burguete J, García-Navarro P, Murillo J. Friction term discretization and limitation to preserve stability and conservation in the 1D shallow-water model: application to unsteady irrigation and river flow. *International Journal for Numerical Methods in Fluids* 2008; **58**(4):403–425.
10. Brufau P, Vázquez-Cendón ME, García-Navarro P. A numerical model for the flooding and drying of irregular domains. *International Journal for Numerical Methods in Fluids* 2002; **39**:247–275.
11. Murillo J, García-Navarro P, Burguete J, Brufau P. A conservative 2d model of inundation flow with solute transport over dry bed. *International Journal for Numerical Methods in Fluids* 2006; **52**:1059–1592.
12. Murillo J, García-Navarro P, Burguete J. The influence of source terms on stability, accuracy and conservation in 2d shallow flow simulation using triangular finite volumes. *International Journal for Numerical Methods in Fluids* 2007; **54**:543–590.
13. Vázquez-Cendón ME. Improved treatment of source terms in upwind schemes for the shallow water equations in channels with irregular geometry. *Journal of Computational Physics* 1999; **148**(2):497.
14. Abbot MB. *Computational Hydraulics*. Ashgate Publishing Company: Vermont, 1992.
15. Burguete J, García-Navarro P, Murillo J, Garcia-Palacin I. Analysis of the friction term in one-dimensional shallow water model: application to open channel and river flow. *Journal of Hydraulic Engineering* (ASCE) 2007; **133**(9):1048–1063.
16. Vázquez-Cendón ME. Implicit and explicit upwind schemes for the 2D shallow water equations in unstructured meshes. *Numerical Modelling of Hydrodynamic Systems*, Zaragoza, 1999; 231–250.
17. Roe PL. A basis for upwind differencing of the two-dimensional unsteady Euler equations. *Numerical Methods in Fluid Dynamics*, vol. II. Oxford University Press: Oxford, 1986.
18. Toro EF. *Riemann Solvers and Numerical Methods for Fluid Dynamics*. Springer: Berlin, 1997.
19. Burguete J, García-Navarro P. Efficient construction of high-resolution TVD conservative schemes for equations with source terms: application to shallow water flows. *International Journal for Numerical Methods in Fluids* 2001; **37**:209–248.

DOI: 10.1002/fld

20. Brufau P, García-Navarro P, Vázquez-Cendón ME. Zero mass error using unsteady wetting/drying conditions in shallow flows over dry irregular topography. *International Journal for Numerical Methods in Fluids* 2004; **45**:1047–1082.
21. Murillo J, García-Navarro P, Burguete J. Analysis of a second-order upwind method for the simulation of solute transport in 2D shallow water flow. *International Journal for Numerical Methods in Fluids* 2008; **56**(6):661–686.
22. Courant R, Isaacson E, Rees M. On the solution of nonlinear hyperbolic differential equations by finite differences. *Communications on Pure and Applied Mathematics* 1952; **5**:243–255.
23. Matsuyama M. Central research institute for electric power industry, Abiko, Japan. *The Third International Workshop on Long-wave Run up Models*, Wrigley Marine Science Center, Catalina Island, California, 2004. http://www.cee.cornell.edu/longwave/index.cfm?page=benchmark\&problem=2 (downloaded 12 April 2007).

DOI: 10.1002/fld